Available online at www.sciencedirect.com
SCIENCE DIRECT®
International Journal of Heat and Mass Transfer 47 (2004) 4559–4568
International Journal of HEAT and MASS TRANSFER
www.elsevier.com/locate/ijhmt

Visualization of boiling structures in high heat–flux pool-boiling

Shigefumi Nishio [a,*], Hiroaki Tanaka [b]

[a] Institute of Industrial Science, The University of Tokyo, 4-6-1 Komaba, Meguro-ku, Tokyo 153-8505, Japan
[b] Sanyo Electric Air Conditioning Co., Ltd., 1-1-1 Sakata, Oizumi-machi, Ora-gun, Gunma 326-8534, Japan

Received 24 April 2003
Available online 26 June 2004

Abstract

The present paper presents experimental results of observation of liquid–solid contact and bubble behaviors around the critical heat flux of saturated and subcooled pool boiling on a plate of single crystal sapphire. The observation was conducted from the backside of a rectangular boiling surface and also from the side and backside of a boiling surface with a narrow width. The main results obtained are summarized as follows. The bubble base area is almost dry and lateral coalescence of bubbles forms coalescent dry areas. As the wall superheat increases, liquid–solid contact becomes like a canal meandering through dry areas. The dependency on the surface superheat of the contact-line length density (CLLD) which is defined as the total length of the boundary between wetted and dry areas in a unit area is almost the same as the boiling curve, and the value of CLLD at CHF is not strongly dependent on boiling liquid and subcooling. The relation of the number density of dry areas and their equivalent diameter in the large dry area region at CHF is not dependent on boiling liquid and subcooling, and it is similar to that of dropwise condensation.

1. Introduction

It is well known that many physical images and models have been proposed for critical heat flux in boiling heat transfer [1], but mechanism triggering the critical heat flux can be grouped into two concepts in general. The first concept assumes that the heat flux itself causes a limit in heat transport and this is named heat–flux governing concept in the present paper. This concept is natural because the heat flux reaches a peak value at the CHF as the word CHF literally means. The types of CHF models based on the heat–flux governing concept are the hydrodynamic instability model proposed by Zuber [2] and the macrolayer depletion model by Haramura and Katto [3]. These models are not directly concerned with the degree of superheat of the boiling surface at the CHF. On the other hand, in the second concept, heat flux is related to the degree of superheat of boiling surface and then the CHF is determined as the peak heat flux. This is named superheat-governing concept. This concept also is natural because the driving force for boiling heat transfer is the degree of superheat. The types of superheat-governing models are the unified-model proposed by Dhir and Liaw [4], the microlayer depletion model of Zhao et al. [5] and the evaporative-meniscus model of Nokolayev et al. [6]. It is known that measurements of CHF can be well described by the empirical equation by Zuber [2]. Although the form of this equation has been successfully derived in the case of the heat–flux-governing models, that is not the case in the case of the superheat-governing models.

Now, if we consider the physical images of vapor bubble and liquid–solid contact structures at the CHF, the hydrodynamic instability model portrays an image, in which: (a) generated vapor escapes from the boiling surface by forming a continuous columnar passage. By contrast, the macrolayer depletion model and the

* Corresponding author. Tel.: +81-3-5452-6172; fax: +81-3-5452-6173.
E-mail addresses: nishios@iis.u-tokyo.ac.jp (S. Nishio), tana021927@sanyo.co.jp (H. Tanaka).

0017-9310/$ - see front matter © 2004 Elsevier Ltd. All rights reserved.
doi:10.1016/j.ijheatmasstransfer.2003.07.033

Nomenclature

$N[D]$	number density of dry area density of diameter D [m^{-2}]	ΔT_{sub}	degree of subcooling of liquid [K]
D	equivalent diameter of dry area [m]	Γ_t	contact-line length density [m/m^2]
q_{CHF}	critical heat flux [W/m^2]	$\Gamma[D]$	$\equiv \int_0^D \gamma[X]dX$
F	time-averaged fraction of liquid–solid contact	$\gamma[D]$	contact-line length density for the dry area in the range of diameters of $D-\Delta D < D < D+\Delta D$ [m/m^2]
ΔT_{sat}	degree of superheat of boiling surface [K]		

unified-model portray a two-layer structure in which (b) a coalesced bubble is formed on the macrolayer attached to the boiling surface (the term macrolayer is used here to distinguish it from microlayer, which is at the bottom of primary bubbles). On the other hand, evaporative-meniscus model assumes (c) a condition in which a vapor bubble contacting with the boiling surface forms an evaporative meniscus that gradually retreats (namely, base of the vapor bubble dries away). The microlayer depletion model assumes both the conditions (b) and (c).

Many of the above models or physical images address only the case of saturated boiling, and therefore, it will be necessary to discuss the possibility of extending the models to include the CHF of subcooled boiling as well [7]. For example, in the physical image (b), it is a prerequisite that a large coalesced bubble exists. However, as the degree of subcooling increases, coalescence of bubbles becomes to be suppressed and average diameter of vapor bubbles on boiling surface becomes significantly smaller even at the CHF condition [8].

Critical heat flux is of great significance in devices such as those that generate vapor and those that use boiling heat transfer to cool a solid surface, but in the present the mechanism triggering the CHF is explained by many deferent models or physical images as stated above. In our point of view, this is mainly due to the following reason: namely, near the CHF, vapor is generated in large amounts making it difficult for one to observe the state of affairs close to the boiling surface. To address this issue, Nagai and Nishio [9,10] attempted to directly observe the state of liquid–solid contacts from behind a boiling surface. The boiling surface that they used was a plate made from a single crystal sapphire, which was transparent and had a thermal conductivity higher than that of stainless steel. That work [10] introduced a concept of contact-line length density Γ_t in which the contact-line length density was defined as the total length of the boundary lines between dry areas and wetted areas (or liquid–solid contact areas) per unit boiling surface area; note that the boundary line can also be called a contact-line or a triple-phase line. The contact-line length density showed a dependency on the degree of superheat, resembling a boiling curve: namely, the contact-line length density attained a peak value at a superheat, which is close to that at the CHF.

Nishio et al. [11] conducted visual observations of vapor bubbles in a pseudo two-dimensional space formed by sandwiching a narrow rectangular horizontal boiling surface between two glass plates. They combined the above results with the visual observations in this pseudo two-dimensional space and proposed a two-layer structure for liquid–vapor structures at the CHF. However, this experiment had some limitations: firstly, structures of liquid–solid contacts and those of vapor bubbles had not been observed simultaneously; secondly, the test liquid was not varied; finally, only the case of saturated boiling was considered.

We believe that the boiling curve is a continuous curve in the high-heat flux boiling region that includes the CHF point; namely, the region that ranges from the high-heat flux nucleate-boiling region to high-heat flux transition-boiling region. In this region, the contact-line length density is a continuous curve resembling the boiling curve, and we believe that this density represents an important index of boiling heat transfer. Incidentally, intensive evaporation takes place near the contact-line or interline [6] formed by vapor bubbles, and we are of the view that the contact-line length density is an index of a spatial density relating to intensive evaporation. The objectives of this work were laid down as follows: collection of experimental data on contact-line length densities by changing the test liquid and liquid temperature as parameters, and making a proposition for the physical image of the CHF phenomenon by simultaneous observations on the liquid–solid contact structures and liquid–vapor structures.

2. Experimental apparatus and method

2.1. Apparatus for visual observation of liquid–solid contacts on horizontal boiling surface

Fig. 1 shows the experimental set-up used in this work. The boiling surface was a mechano-chemically polished surface of a single crystal sapphire plate that

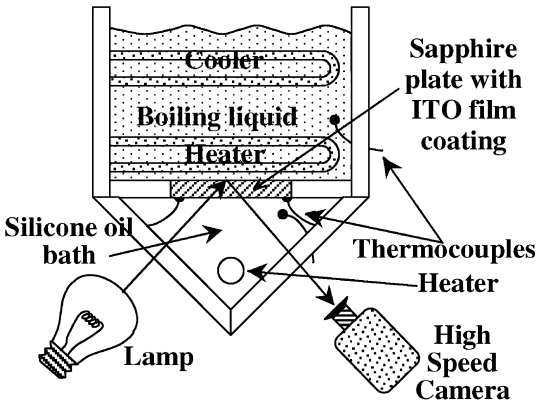

Fig. 1. Experimental setup for observation of liquid–solid contact on horizontal flat plate.

was a square of 40 mm width and 3 mm thickness. The roughness of the boiling surface was not measured in this experiment, but it can be expected that its maximum roughness to be 0.04 μm and that its central-average roughness to be 0.004 μm [12], because we used a polishing procedure identical to our previous works [9,10]. The sapphire plate was coated from the backside with a transparent conductive layer (ITO layer), through which an electrical direct current was passed to heat the sapphire boiling surface. This heat-transfer surface assembly was placed at the bottom of a boiling vessel, and boiling experiments were performed at one atmosphere for the horizontal upward-facing orientation of the boiling surface. The test liquids of the experiments were R113, R141b and ethanol. For R113, only saturated boiling experiments were done; for R141b, experiments were extended up to a degree of subcooling, $\Delta T_{sub} = 30$ K and for ethanol, up to $\Delta T_{sub} = 40$ K. A triangular prism, which was fitted at the bottom of the boiling vessel and filled with a silicone oil, allowed visual observations of the liquid–solid contacts on the boiling surface to be made from behind the boiling surface (to be described in detail later).

In the experiments, the electrical current to ITO layer located on the backside of sapphire boiling surface was increased one step at a time, and for each value of current a boiling experiment was done. In the steady-state, the heat flux q at the boiling surface was obtained from the electrical current. To find the degree of superheat of the boiling surface ΔT_{sat} in this case, first the backside temperature of the boiling surface was obtained from the ITO layer's resistance, which was precalibrated for temperature dependency. Next, using a steady-state heat conduction equation, the temperature drop across the sapphire-plate thickness was calculated. In the transition boiling region, both the degree of superheat and heat flux of the boiling surface were obtained by using the history of transient temperature rise of the ITO layer and the inverse method of heat conduction calculations [10]. For reference purpose, a thermocouple (of K-type and 0.1 mm diameter) glued to the ITO layer was also used. To reduce heat loss to the silicone oil bath, silicone oil temperature was adjusted so that it was identical to the backside temperature of boiling surface at the steady state. In the transition boiling region, the silicone oil temperature was maintained at the CHF temperature. Using the total reflection method [9,10], the state of liquid–solid contacts was recorded for each of the conditions by using a high-speed video camera at 1000 frames/s (or 500 frames/s depending on the case).

2.2. Experiment for simultaneous observation of states of liquid–solid contacts and vapor bubbles in pseudo two-dimensional boiling space

To examine the correspondence between the state of liquid–solid contacts and that of vapor bubbles, we conducted boiling experiments in a pseudo two-dimensional space. The experimental set-up is shown in Fig. 2. Both the experimental set-up and procedure are almost identical to those described in Section 2.1, and only the differences are described below. The boiling surface was a single crystal of sapphire having a 1 mm width, 80 mm length and 3 mm thickness, and its surface was mechano-chemically polished. The boiling surface was sandwiched between two vertical glass plates, each 2 mm in width and 1 mm in height (to the top of the glass plate from the boiling surface) to form a pseudo two-dimensional boiling space of 1 mm gap. This heat transfer surface assembly was fixed at the bottom of a boiling vessel. We conducted boiling experiments at one atmosphere with the heat transfer surface in horizontal upward-facing orientation. In the experiments, test liquid

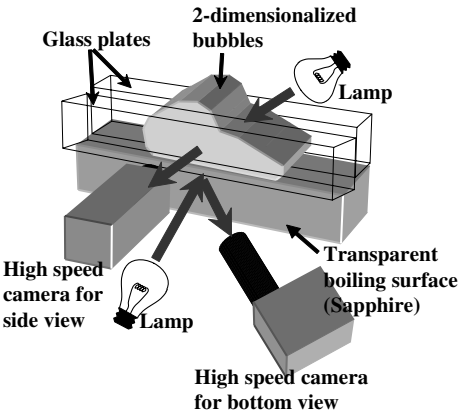

Fig. 2. Experimental setup for observation of bubble and liquid–solid contact structures in quasi-two-dimensional boiling space.

was R141b, and liquid sub-cooling was varied up to 30 K. Using two high-speed video cameras, we recorded the state of liquid–solid contacts and that of bubbles simultaneously at 500 frames/s. For recording the state of liquid–solid contacts, we used the total reflection method from behind the boiling surface, and for recording the state of vapor bubbles, we used backlight-method by the light passing through the glass plates. These two images were combined into a single frame.

2.3. Image processing

To identify the liquid and vapor areas in contact with the boiling surface, we processed the video images obtained in the experiment as follows. We chose a square area whose side was equal to the wavelength of Taylor instability, and we converted the images in the area into binary images of black and white for a period of 100 ms; note that the Taylor wavelength is 13 mm for R141b and 17 mm for ethanol. Incidentally, the ratio of observation time to the departure period [2] of coalesced bubbles at the CHF is 1.7 for ethanol, 2.4 for R113, and about 2.2 for R141b. Similarly, the ratio of the length of a side of the observation area to departure diameter of a coalesced bubble [2] is 0.77 for ethanol, 1.1 for R113 and 0.83 for R141b. We also conducted an experiment to perform visual observations from the backside of the boiling surface using the polarized method [13]. Since the results of the experiments were similar to the images obtained with the total-reflection method, we decided that bright areas in the binary images represented dried out areas. From a binary image, we calculated such factors as the fraction of liquid–solid contacts F, the contact-line length density Γ_t and the equivalent diameter D and number density $N[D]$ of dry areas.

3. Results of state of liquid–solid contacts

This section describes the results we could derive regarding the state of liquid–solid contacts, from the images obtained with the experimental apparatus described in Section 2.1.

3.1. Patterns of liquid–solid contacts

Fig. 3 shows typical images of liquid–solid contacts obtained in the present work for saturated boiling of ethanol. The figure illustrates how the patterns of liquid–solid contacts have changed when the degree of superheat was increased. The patterns of liquid–solid contacts observed are as follows: a planar solid–liquid contact (at $\Delta T_{sat} = 25$ K), which include isolated circular dry areas; a planar liquid–solid contact (at $\Delta T_{sat} = 28$ K), which included coalesced dry areas; a network of liquid–solid contacts like a canal meandering between dry areas (at $\Delta T_{sat} = 33$K), which had a broad diameter distribution; and a network of liquid–solid contacts (at $\Delta T_{sat} = 46$ K), which included isolated wetted area in a large dry area. Similar patterns were observed in the case

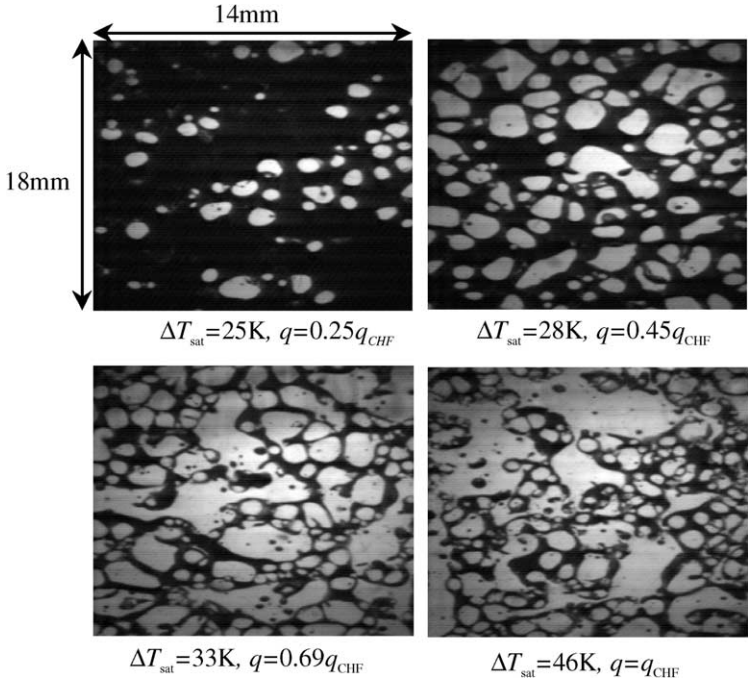

Fig. 3. Typical images of liquid–solid contact of saturated ethanol on horizontal flat plate.

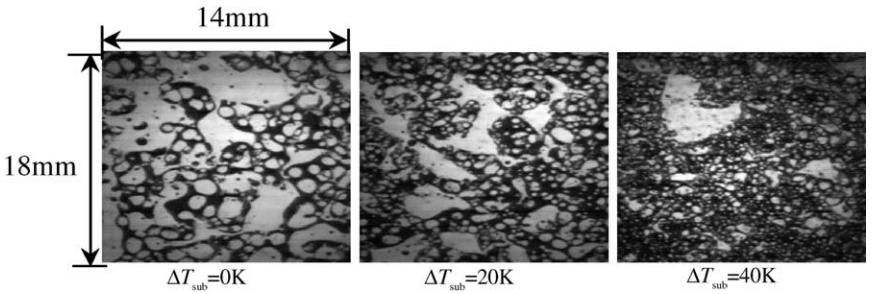

Fig. 4. Effect of liquid subcooling on liquid–solid contact pattern at critical heat flux of ethanol.

of R113 [11], and similar results were obtained in the present work for R141b. Therefore, we were of the view that the patterns of liquid–solid contacts described above would occur irrespective of the fluid.

Fig. 4 shows how liquid subcooling affects the state of liquid–solid contacts at CHF in the case of ethanol. With an increase in the liquid subcooling, the number density of large dry areas would decrease; conversely, the number density of small dry areas would increase. However, the pattern of the network of liquid–solid contacts can be thought of as remaining intact.

3.2. Fraction of liquid–solid contacts

The fraction of liquid–solid contacts F is a quantity often used to describe the characteristics of boiling in the transition-boiling region. Therefore, for the case of saturated boiling, the present experimental data of the spatially and time averaged fraction of liquid–solid contact were shown in Fig. 5 together with those in the literature [14–18]. The abscissa is the surface superheat scaled by the superheat at CHF. It is seen from the figure that the liquid–solid contact fractions at the CHF obtained in the present experiments are less than 40%. These low contact-fractions can be attributed to the fact that the nucleate boiling curve shifted to a high superheat region because the boiling surface was very smooth and pre-existing vapor nuclei on the surface were limited to smaller ones. It should be noted that, as shown in Fig. 9 to follow, the values of CHF of the present experiment are somewhat smaller than the values obtained from Zuber's equation [2] but the differences are not significant. For the CHF conditions of ethanol and R141b, we have shown in Figs. 6 and 7 the dependence of F and other characteristic quantities on degree of subcooling. From these figures, it can be seen that F increases roughly linearly with respect to the degree of subcooling.

3.3. Boiling curve and contact-line length density

The contact-line length density Γ_t is a concept that is completely different from the concept of liquid–solid

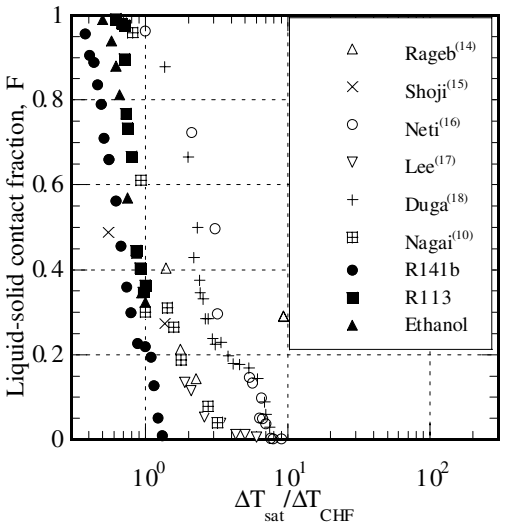

Fig. 5. Liquid–solid contact fraction.

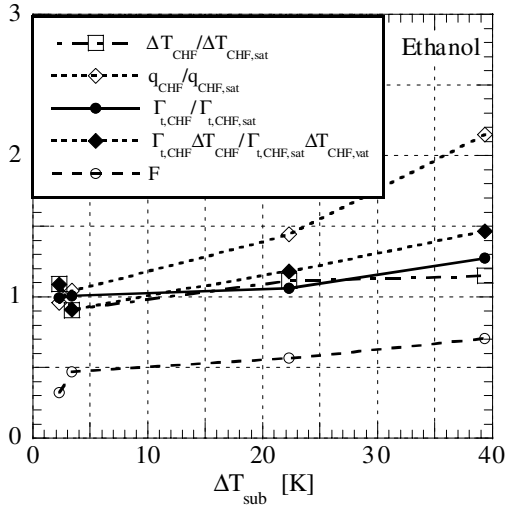

Fig. 6. Effect of liquid subcooling on characteristic values of boiling of ethanol.

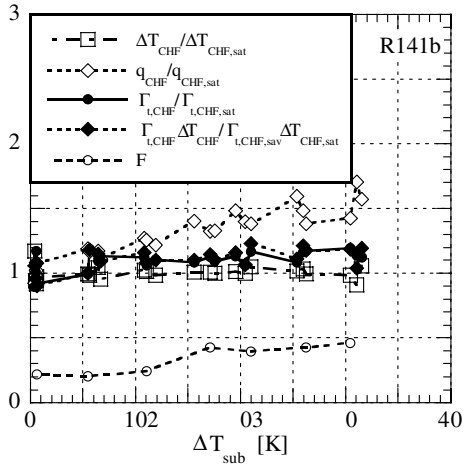

Fig. 7. Effect of liquid subcooling on characteristic values of boiling of R141b.

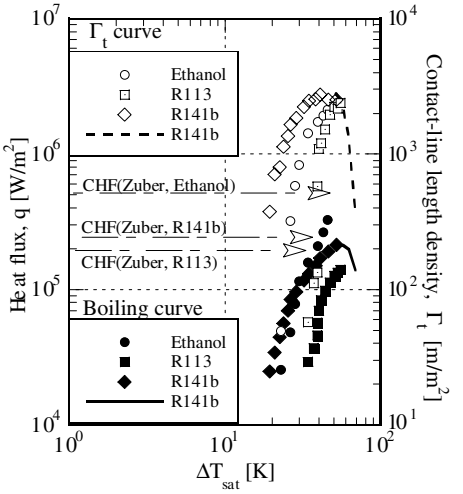

Fig. 9. Superheat dependence of boiling heat transfer and contact-line-length density of saturated boiling.

contact fraction F. For example, we consider the following two cases; namely, a large dry area per unit area with $F = 0.25$ and four dry areas of half the previous diameter. The value of Γ_t for the latter case will be two times that of the former case although F is the same. Fig. 8 shows time variations of the contact-line length density for saturated boiling of ethanol; the parameter in the figure is the heat flux scaled by CHF. This figure shows that, at least in the case of saturated boiling, the time variation of Γ_t is not so large. Therefore, we shall focus on the average value of Γ_t in the discussions to follow. Incidentally, Γ_t at CHF is of the order of a few km/m^2.

Fig. 9 shows a comparison between the boiling curve and the curve representing the dependence of contact-line length density on the degree of superheat for each of the three saturated liquids used in the present experiment. For R141b, the data in the transition boiling region are shown by a dashed line and a solid-line. The values of CHF for each of the liquids using Zuber's equation also are shown. If the experimental data of CHF are compared with the values predicted from the Zuber's equation, the experimental data are lower than the predictions by 30% for ethanol, by 20% for R113 and by 10% for R141b. Although this paper does not intend to discuss details of these differences, the difference can be attributed to effects of thermal properties of the boiling-surface material [19]. The contact-line length density Γ_t increases with respect to the degree of superheat for each of the liquids considered. In addition, in the case of R141b, it decreases with respect to the degree of superheat in the transition-boiling region as shown. Therefore, the relationship between contact-line length density and degree of superheat has a striking resemblance to a boiling curve.

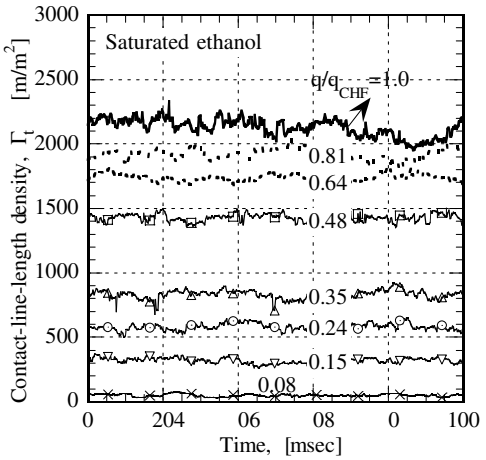

Fig. 8. Fluctuation of contact-line length density of saturated ethanol.

Incidentally, a conclusion drawn in the references [10] and [11] for R113 was that the contact-line length density was an important index in boiling heat transfer. The deduction to be made from the above is that this conclusion is a valid statement for other liquids as well. In addition, to be noted is the fact that the values of the contact-line length density at CHF for the liquids are close to each other and that they lie roughly between 2 and 3 km/m^2, even though the values of CHF for the three liquids are very different from each other.

3.4. Diameter distribution of dry areas

Using the images shown in Figs. 3 and 4, we calculated a diameter D of each circle that was equivalent in

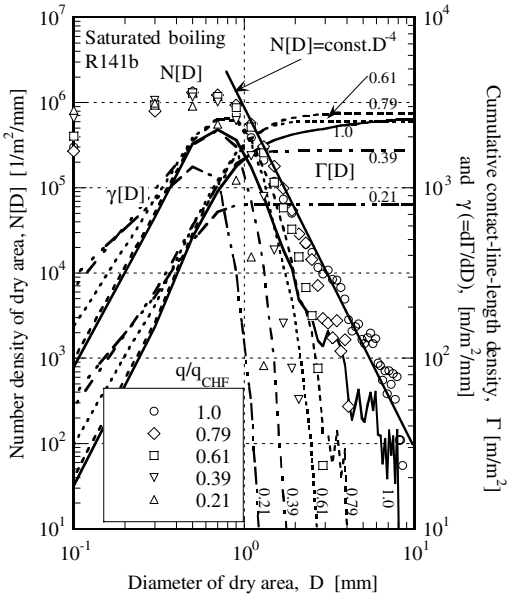

Fig. 10. Dependence of $N[D]$, $\gamma[D]$ and $\Gamma[D]$ on heat flux for saturated R141b (the symbols denote experimental data of $N[D]$, the lines monotonically increasing denote values of $\Gamma[D]$, and the lines having maximum denote values of $\gamma[D]$, the number attached each line is the value of q/q_{CHF}).

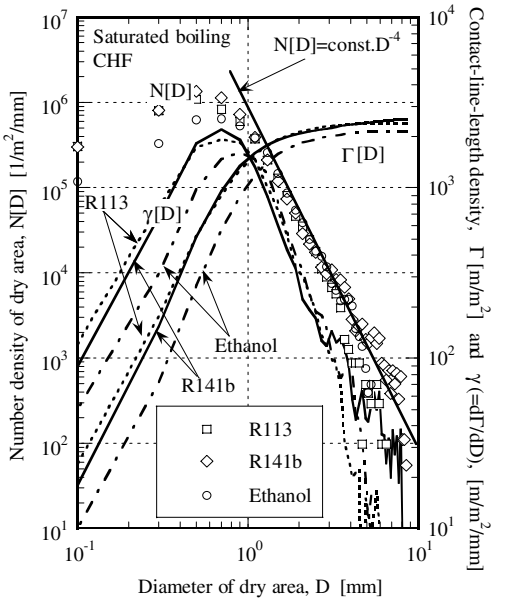

Fig. 11. Characteristic values of dry areas at CHF of saturated boiling (the symbols denote experimental data of $N[D]$, the lines monotonically increasing denote values of $\Gamma[D]$, and the lines having maximum denote values of $\gamma[D]$).

area to each dry area in the images. The number density of dry areas $N[D]$ was defined as the number of dry areas per unit area in the diameter range, $D-\Delta D<D<D+\Delta D$, where $\Delta D=0.1$ mm. This density is plotted in Fig. 10 for saturated R141b with heat flux as the parameter. The figure also shows distributions of the contact-line length density $\gamma[D]$ for the dry areas within each of the diameter ranges and its integral $\Gamma[D]=\int_0^D \gamma[D]\mathrm{d}X$. The figure shows that there are two distinctive dry-area regions: namely, a region of small diameters in which $N[D]$ increases gradually with respect to D, and a region of larger diameters in which $N[D]$ decreases with respect to D. We believe that the small-diameter region corresponds with the primary dry area region [10,11] that are not coalesced, and that the large-diameter region corresponds with the coalesced dry area region.

As seen from Fig. 10, the lower-limit diameter of large-diameter region gradually increases when the heat flux increases. If the relation between $N[D]$ and D in the large-diameter region is expressed as $N[D]\propto D^{-m}$, the value of m increases with increasing heat flux and approaches a constant about 4 as CHF is approached. As in Fig. 10, each of the above quantities at CHF of saturated boiling was shown in Fig. 11 for the three liquids. Each distribution $N[D]$, $\gamma[D]$ and $\Gamma[D]$ for a given liquid has a close similarity with those for other liquids. Especially, it was found that the dry-area diameter distribution in the large diameter region to be falling onto an identical line for each of the fluids, this line having roughly a gradient $m=4$.

Figs. 12 and 13 show the effects of subcooling on the above quantities for R141b and ethanol. First, for the small-diameter region defined above for saturated boiling, the number density of dry areas increases with an increase in the liquid subcooling as mentioned in Section 3.1 and the dry-area distribution curve acquires a negative gradient. However, the dry-area diameter distribution in the large diameter region at CHF will fall onto the identical line that has roughly a gradient $m=4$ even in the case of subcooled boiling as in saturated boiling. It should be noted that the number density of dry areas of larger diameters in the large-diameter region decreases with an increase in the degree of subcooling. This is the reason why the liquid–solid contact fraction increases with respect to liquid subcooling as shown in Figs. 6 and 7.

From the above facts, we can deduce that there is a close relationship between the facts that the dry-area diameter distribution attains the approximate relationship, $N[D]\propto D^{-4}$ in the large-diameter region and that the CHF is attained as a result of the liquid–solid contacts being limited to a network of contacts. This is an interesting result in considering the fact that the approximate relationship [20], $N[D]\propto D^{-3.87}$ is valid in relatively large droplet-diameter range in drop-wise condensation, where the fundamental mechanism of

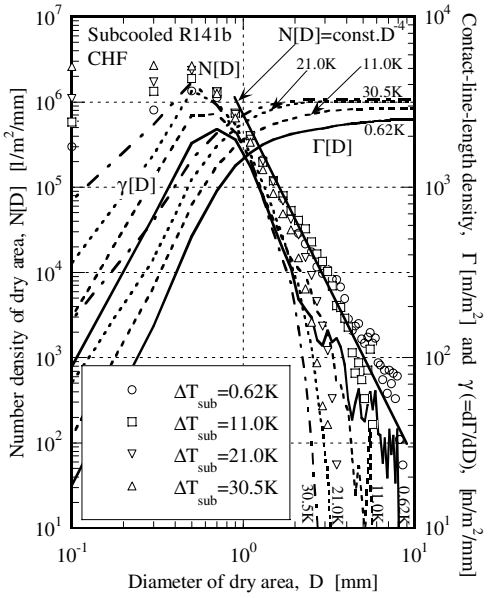

Fig. 12. Effect of subcooling on characteristic values of dry areas at CHF of R141b (the symbols denote experimental data of $N[D]$, the lines monotonically increasing denote values of $\Gamma[D]$, and the lines having maximum denote values of $\gamma[D]$, the number attached each line is the degree of subcooling).

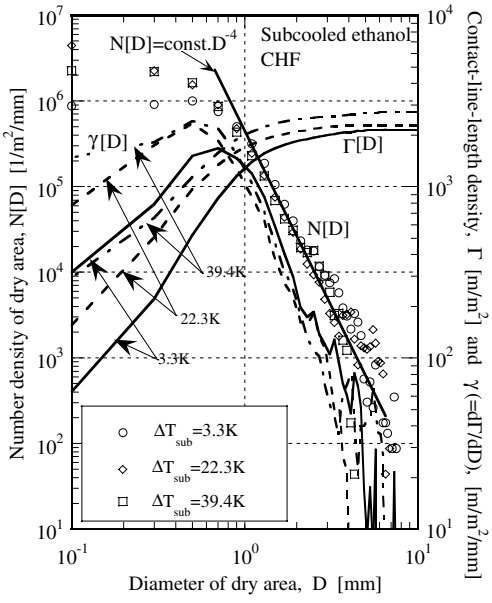

Fig. 13. Effect of subcooling on characteristic values of dry areas at CHF of ethanol (the symbols denote experimental data of $N[D]$, the lines monotonically increasing denote values of $\Gamma[D]$, and the lines having maximum denote values of $\gamma[D]$, the number attached each line is the degree of subcooling).

heat transfer phenomenon is the process of coalescing of droplets.

3.5. Contact-line length density

Figs. 10–13 also show the distributions of $\gamma[D]$ and $\Gamma[D]$. As can be easily deduced from the dry-area diameter distribution, the distribution of $\gamma[D]$ has a peak value for all the cases shown, and the value of D_m that corresponds with the maximum of $\gamma[D]$ decreases when the liquid subcooling increases. As stated in reference [21], D_m is close to the dry area diameter D_s which can be derived using a close-packed condition for dry areas and an instantaneous nucleation density (namely, the density of nuclei that generate vapor bubbles at a particular instance) at CHF. On the other hand, $\Gamma D = 10$ mm] that is shown in Figs. 10–13 is close to Γ_t, which increases gradually with respect to liquid subcooling although the dependence is small. Incidentally, within the scope of the present experiments, the minimum value of Γ_t at CHF was 2.1 km/m^2 in the case of saturated ethanol, and the maximum value was 3.2 km/m^2 in the case of R141b at $\Delta T_{sub} = 30.5$ K.

4. Results on relationship between state of liquid–solid contacts and state of vapor bubbles

Based on the visual images obtained with the experimental set-up of Section 2.2, we shall present in this section, experimental results to show the relationship between the states of liquid–solid contacts discussed in Section 3 and the states of vapor bubbles.

4.1. Structure of vapor bubbles

Fig. 14 shows a typical observation result for R141b, under saturated nucleate boiling at a high heat flux ($q = 0.77 q_{CHF}$). In each of the frames in the figure, section

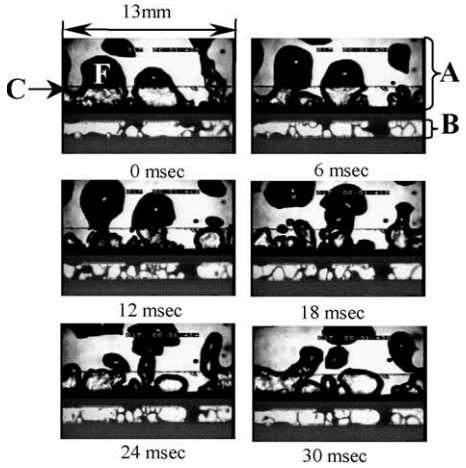

Fig. 14. Typical pictures of bubble and liquid–solid contact structures of saturated R141b at $q = 0.77 q_{CHF}$.

A represents an image from the sideways of the boiling surface, and section B represents an image from the back side of the boiling surface. The horizontal line represented by C is the top edge of the vertical side-glass plate.

First, if we compare the states of sections A and B, we can see that the base area of each vapor bubble is almost dried up and as a result the liquid–solid contacts are limited to narrow regions among the bubbles. This situation has resulted in the appearance of a network of liquid–solid contacts as mentioned in Section 3.1. Now, it is clear that the dry areas discussed in Section 3 correspond with the base areas of vapor bubbles. Also it should be noted that the coalesced vapor bubble F shown in the image at $t = 0$ ms is detached at a time $t < 12$ ms, and that both a small vapor bubble and a small dry area have appeared at that location as can be seen from the frames at $t = 12$ and 18 ms. Then, the bubbles coalesce themselves in the horizontal direction, and the coalesced bubble would grow as can be seen from the frames at $t = 24$ and 30 ms. Namely, in the high-heat flux boiling, each vapor bubble has a base that is almost dried up, and the vapor bubbles coalesce with the neighboring bubbles in the horizontal direction to form a coalesced bubble, which creates a coalesced dry area. This image is different from the image of boiling near CHF as portrayed by the macrolayer depletion model, which assumes a layered-structure consisting of a coalesced vapor bubble and a macrolayer.

4.2. Effect of heat flux and degree of subcooling on structure of vapor bubbles

Fig. 15 shows the states of both vapor bubbles and liquid–solid contacts for boiling of R141b in the pseudo 2-dimensional boiling space at several scaled heat fluxes (q/q_{CHF}) with respect to several values of liquid subcooling.

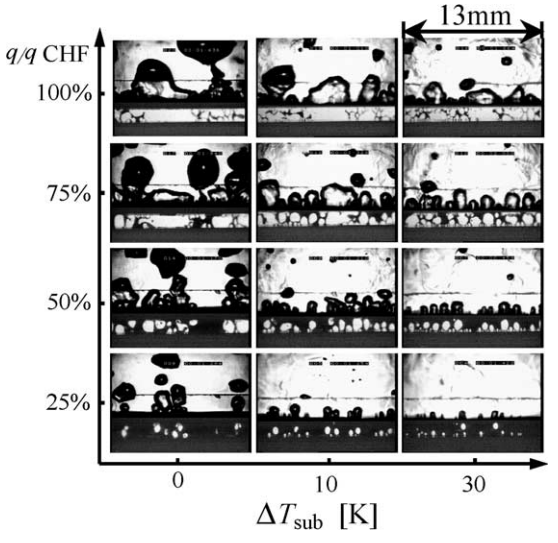

Fig. 15. Effects of heat flux and subcooling on bubble and liquid–solid contact structures of R141b.

First, considering effects of subcooling at a given value of scaled heat flux, we can see that vapor bubble diameter gets smaller when the subcooling is increased, as we have reiterated. However, bases of the bubbles are almost dried up even in subcooled boiling as in saturated boiling. Although not shown in the figure, even at $\Delta T_{sub} = 30$ K, primary vapor bubbles are involved in forming coalesced vapor bubbles by way of sliding on the boiling surface and absorbing neighboring vapor bubbles. Namely, even in the case of subcooled boiling, it was clear that vapor bubbles get coalesced in the horizontal direction to form coalesced vapor bubbles and coalesced dry areas.

5. Conclusions

In this work, visualization experiments were done to observe the state of liquid–solid contacts and the state of vapor bubbles under high-heat flux boiling in saturated and subcooled liquids. The followings are the conclusions drawn.

1. In high-heat flux boiling, the base area of each vapor bubble becomes almost dried up, and this base area of a bubble represents a dry area. Therefore, in high-heat flux boiling, liquid–solid contacts are limited to the narrow regions bounded by the vapor bubbles, thus forming a liquid–solid contact pattern of a network.
2. Whether it is saturated boiling or subcooled boiling, formation of a coalesced bubble and a coalesced dry area will take place when a vapor bubble combines with an adjacent vapor bubble in the horizontal direction.
3. It was shown by performing experiments covering nucleate to transition boiling that the contact-line length density attained a peak value near CHF in saturated boiling of R141b, just as in saturated boiling of R113. It was also shown that there was a resemblance between the dependence of contact-line length density on the surface superheat and the boiling curve. This fact suggests that the contact-line length density is an important concept in describing boiling heat transfer in the high-heat flux region.
4. Within the scope of the present series of experiments, the contact-line length density at CHF has a weak dependence both on the kind of boiling liquid and the degree of subcooling.
5. Number density $N[D]$ of dry areas in the large-diameter region at CHF, where the dry areas are the coalesced dry areas, falls onto a single line of $N[D] \propto D^{-4}$, irrespective of the kind of boiling liquid

or the degree of subcooling. This relation is close to that of the droplet diameter distribution in drop-wise condensation, where the process of droplet coalescing is the fundamental mechanism behind the heat transfer phenomenon.

References

[1] S.G. Kandlikar, A theoretical model to predict pool boiling CHF incorporating effects of contact angle and orientation, ASME J. Heat Transfer 123 (2001) 1071–1079.

[2] N. Zuber, Hydrodynamic aspects of heat transfer, Ph.D. thesis, UCLA, 1959.

[3] Y. Haramura, Y. Katto, New hydrodynamic model of critical heat flux applicable widely to both pool and forced convective boiling on submerged bodies in saturated liquids, Int. J. Heat Mass Transfer 26 (1983) 379–399.

[4] V.K. Dhir, S.P. Liaw, Framework for a unified model for nucleate and transition pool boiling, ASME J. Heat Transfer 111 (1989) 739–746.

[5] Y.-H. Zhao, T. Masuoka, T. Tsuruta, Prediction of critical heat flux based on the microlayer model, Trans. JSME (in Japanese) 62B (1996) 2338–2343.

[6] V.S. Nikolayev, D.A. Beysens, G.-L. Laier, J. Hegseth, Growth of a dry spot under a vapor bubble at high heat flux and high pressure, Intern. J. Heat Mass Transfer 44 (2001) 3499–3511.

[7] Y.-H. Zhao, T. Masuoka, T. Tsuruta, Critical heat flux of subcooled pool boiling based on the microlayer model, Trans. JSME 67B (2001) 466–472.

[8] S. Nishio, H. Tanaka, H. Asou, Bubble structures in high-heat–flux subcooled pool-boiling, Therm. Sci. Eng. 11 (2003).

[9] N. Nagai, S. Nishio, A method for measuring the fundamental quantities on liquid–solid contact in pool boiling using an image processing technique, Proc. ASME Fluids Engineering Division Summer Meeting (Flow Visualization and Image Processing of Multiphase Systems), ASME FED-vol. 209, 1995, pp. 73–79.

[10] N. Nagai, S. Nishio, Study of the liquid–solid contact phenomena in boiling heat transfer (proposal of concept of contact-line length density), Proc. of the First Pacific Symposium on Flow Visualization and Image Processing, (Honolulu) 2, 1997, pp. 469–474.

[11] S. Nishio, T. Gotoh, N. Nagai, Observation of boiling structures in high heat–flux boiling, Intern. J. Heat Mass Transfer 41 (1998) 3191–3201.

[12] N. Nagai, Liquid–Solid Contact Phenomena in Boiling Heat Transfer on Extremely Smooth Surface of Single Crystal Sapphire with Visualization Technique, Dr. Eng. Thesis, The University of Tokyo, 1996.

[13] R.R. Sharp, The nature of liquid film evaporation during nucleate boiling, NASA TN D-1997 (1964).

[14] H.S. Ragheb, S.C. Cheng, Surface wetted area during transition boiling in forced convective flow, ASME J. Heat Transfer 101 (1979) 381–383.

[15] S. Shoji, M. Kawakami, Study of heat transfer mechanism and surface temperature fluctuation in transition and film boiling, Proc. 26th National Heat Transfer Symposium of Japan (in Japanese) 3, 1989, pp. 806–808.

[16] S. Neti, T.J. Butrie, J.C. Chen, Fiber-optic liquid contact measurements in pool boiling, Rev. Sci. Instrum. 57 (1986) 3043–3047.

[17] L.Y.W. Lee, J.C. Chen, Liquid–solid contact measurements using a surface thermocouple temperature probe in atmospheric pool boiling water, Intern. J. Heat Mass Transfer 28 (1985) 1415–1423.

[18] D.S. Dhuga, R.H.S. Winterton, Measurement of surface contact in transition boiling, Intern. J. Heat Mass Transfer 28 (1985) 1869–1880.

[19] A.A. Watwe, A. Bar-Cohen, The role of thickness and thermal diffusivity in pool boiling CHF in highly-wetting liquids, Heat Transfer 5 (1996) (1994) 183–188.

[20] I. Tanasawa, Drop-wise condensation, Progress in Heat Transfer Engineering (in Japanese), Youkendo, Tokyo, 4, 1976, 301.

[21] S. Nishio, H. Tanaka, Simplified model predicting contact-line-length density at critical heat flux based on direct observation of boiling structure, JSME Int. J. Ser. B 45 (2002) pp. 72–78.